

Quantifying the Upper Limit of Backflash Attack in Quantum Key Distribution

Jialei Su,^{1,2} Junxuan Liu,² Zihao Chen,² Mingyang Zhong,² Qingquan Peng,² Jiangfang Ding,² Yijun Wang,^{1,*} Anqi Huang,^{2,†} and Ying Guo³

¹*School of Automation, Central South University, Changsha 410083, China*

²*Institute for Quantum Information & State Key Laboratory of High*

Performance Computing, College of Computer Science and Technology,

National University of Defense Technology, Changsha 410073, People's Republic of China

³*School of Computer, Beijing University of Posts and Telecommunications, Beijing 100876, China*

(Dated: January 20, 2025)

Quantum Key Distribution (QKD) theoretically provides information-theoretic security based on physical laws. However, imperfections in practice lead to the possibility of quantum hacking on the QKD implementation, especially the passive attacks that are difficult to be detected. In this paper, we study experimentally and theoretically the upper limit of a backflash attack, as one of the vital passive attacks, on a fiber-based QKD system. We experimentally demonstrate the backflash attack on a full equipped fiber-based QKD receiver to show its feasibility and limited distinguish ratio of decoding. More importantly, we have developed a simulation model to analyze the maximum distinguish ratio of decoding can be achieved considering the wide-spectrum feature of backflash photons, which indicates that Eve can extract effective key information from 95.7% of the backflash photons. Consequently, the secure key rate of the decoy-state BB84 QKD system under backflash attack is calculated. This work provides a general methodology to comprehensively evaluate the effect of the backflash attack on a QKD system.

I. INTRODUCTION

The evolution of quantum computing has presented a significant challenge to cryptographic algorithms whose security depends on computational complexity [1]. Research indicates that quantum computers have the potential to effectively break traditional encryption algorithms such as RSA [2]. Fortunately, the quantum key distribution (QKD), which provides a solution based on the laws of quantum physics, shares symmetric secret keys between two parties and offers information-theoretic security against eavesdropping [3–5]. However, in practice, achieving an unhackable QKD system is a challenging task due to the imperfect devices that can be exploited by an eavesdropper (Eve) to learn secret key information [6–16].

Regarding the security of the receiver (Bob) in a prepare-and-measure QKD system, Eve can exploit the imperfections of the detectors to eavesdrop on the secret key. For example, various loopholes on the receiver side were discovered, such as the blinding attack [7, 12, 17, 18], the after-gate attack [19], and the time-shift attack [20]. These attacks on single photon avalanche detectors (SPADs) are active ones that require intercept-resend the quantum states or modulate the light sent to the receiver via the channel. As a result, Eve's actions always induce alterations in the parameters of a QKD system, such as the quantum bit error rate (QBER), the gain of signal states, or the photocurrent of the detectors. These changes in the system's parameters and status allow the attacks to be detected.

Compared to active attacks, passive attacks are relatively hard to be detected. Backflash attack is a typical passive attack of SPAD, in which Bob's SPAD probabilistically generates backflash photons when a detection avalanche occurs [21–24]. These backflash photons transmit backward to the quantum channel and carry the information of the secret key. Then Eve places a copy of Bob's apparatus in the quantum channel to perform the same measurement as Bob on backflash photons to decode the original quantum state. In the backflash attack, Bob emits backflash photons, and Eve only passively receives the backflash photons without causing any changes to the system's parameters. From this aspect of view, the backflash attack is of significant concern for practical QKD systems.

As early as 1956, the emission of secondary photons in p-n junctions was discovered [25]. In recent years, backflash has been considered in QKD systems. Reference [23] analyzed the number of backflash photons generated by a stand-alone SPAD through optical fiber. Additionally, they provided a method for measuring the wavelength of backflash photons to obtain its approximate spectrum, which presents the wide-spectrum property. However, this study did not test backflash attacks in the scenario of an actual fiber-based QKD system. Regarding free-space QKD systems, the backflash attack was demonstrated in Ref. [24], although only the horizontal polarization state $|H\rangle$ and the vertical polarization state $|V\rangle$ are detected with limited distinguished ratio. Regardless of whether in free-space or fiber-based QKD systems, Eve's ability of distinguishing the quantum states that carry key information by the backflash photons is still uncertain. Specifically, the reason of the limited distinguished ratio is unclear, which results in the unknown upper limit of the distinguishing ability. Moreover, this

* xxywyj@sina.com

† angelhuang.hn@gmail.com

limited distinguished ratio has not been considered in the security proof to estimate the leaked key information.

This work studies the backflash attack on a polarization-encoding fiber-based QKD system, quantifying the upper limit of this attack to obtain the information of secret key. We experimentally verified Eve's ability to decode backflash photons in this QKD systems and perform a quantitative analysis of backflash photon counts. In the testing, it is observed that the extinction ratio of distinguishing polarization states in an orthogonal basis is only up to 28.3, with 23.4 as average. To study the reason of the limited extinction ratio, we modeled the optical components used in the experiment and performed theoretical simulations of Eve's decoding process by considering the wide-spectrum property of backflash photons, which shows the upper limit of her ability to distinguish the quantum states of backflash photons, matching to the experimental results. Finally, the limited extinction ratio in practice is taken into account to evaluate the information leakage rate caused by the backflash, and consequently the secure key rate under the backflash attack is simulated.

The paper is structured as follows. We first introduce the experimental scheme and the testing procedure for the backflash attack in Sec. II. The experimental results are shown in Sec. III. Section IV presents the simulation model and methodology to theoretically verify the limited extinction ratio of the decoding polarization states. In Sec. V, the key rate has been simulated based on the information leakage ratio considering the limited extinction ratio of Eve's decoding. Finally, we discuss the effects of this attack and conclude in Sec. VI.

II. EXPERIMENTAL SETUP AND TEST PROCEDURE

A. Experimental setup

The experiment aims to investigate Eve's capability to learn the information of secret key through backflash photons in QKD systems. The experimental setup simulates a backflash hacking scenario in which Eve eavesdrops on a fiber-based QKD system. The testing schematic is shown in Fig. 1.

On Alice's side, the laser diode is configured to emit pulse laser light at the wavelength of 1550 nm, with the intensity attenuated to the single-photon level by an optical attenuator. A polarization controller (PC) is employed to modulate the polarization states of the emitted photons as encoding. On Bob's side, PC2 is used to compensate for the polarization drift of the photons transmitted through the channel, enabling SPAD1 and SPAD2 to accurately detect the signal photons. Bob's detector (IDQ-ID210) is set to external-gating mode, triggered by 100 kHz electrical pulses. To minimize the dark count rate, the dead time is set to 9.8 μ s, resulting in a dark count rate of approximately 50 Hz. To enhance the de-

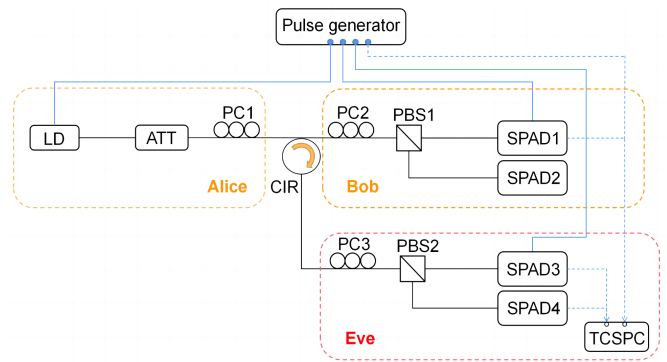


FIG. 1. Experimental setup. The black solid lines represent optical fibers, the blue solid lines indicate cables used for triggering devices, and the blue dashed arrows depict the electrical signals transmitted to the time-correlated single photon counting (TCSPC). LD, laser diode; ATT, optical attenuator; PC, polarization controller; CIR, optical circulator; PBS, polarization beam splitter; SPAD, single photon avalanche detector.

tection probability of a single photon, the gate width is set to 15 ns.

Once SPAD1 or SPAD2 registers a click, it generates backflash photons simultaneously, which are routed through an optical circulator to Eve. The SPADs used by Eve to detect the backflash photons are the same model as Bob's. To maximize the decoding of the backflash photon, Eve employs PC3 as polarization calibration. The TCSPC is employed to register the detection events of Eve's detection click. The pulse generator provides electrical synchronization signal, to trigger the laser diode, the SPADs, and the TCSPC. The experiment is performed at the repetition rate of 100 kHz.

B. Test procedure

To ensure that Eve correctly decodes the quantum states of backflash photons, it is necessary to calibrate Eve's PC before the test. For this purpose, a 1550 nm laser beam is emitted from the position of SPAD1 to the reverse direction of quantum-state transmission, entering the receiver unit through on the slow axis of PBS1. By adjusting PC3, the detection probability of SPAD3 is maximized while that of SPAD4 is minimized, resulting in the extinction ratio of approximately 1000. In this way, Eve decodes the polarization state based on the backflash photons to mostly align with the polarization state detected by Bob. That is, when Bob's SPAD1 and SPAD2 detect the $|H\rangle$ and $|V\rangle$ states separately, Eve's SPAD3 and SPAD4 decode the corresponding quantum states of the backflash photons respectively. For the other set of diagonal basis, we calibrate the setup using the same method.

In the experiment, Alice repeatedly emits optical pulses encoded to one of four polarization states ($|H\rangle$),

$|V\rangle$, $|A\rangle$, $|D\rangle$), which are decoded by Bob and detected via his SPADs. Eve’s SPADs are set to different modes in two tests denoted as Test1 and Test2. In Test1, to observe the distribution of backflash photons over a period of time, Eve’s SPADs are configured to operate in the free-running mode. A 100 kHz clock signal from the pulse generator is sent to the START channel of the TCSPC, while the detection output of Eve’s SPAD3/SPAD4 ($|H\rangle$ or $|V\rangle$) is connected to the STOP channel of the TCSPC.

In Test2, to count the number of backflash photons, Eve’s SPADs are set to operate in the external-gating mode, where the time window of the triggered gate should encompass the time that the backflash photon reaches the SPAD. It is necessary to register coincidence counts within a specific time window to exclude backreflection events. The detection signal from Bob’s SPAD1 or SPAD2 is routed to the START channel of the TCSPC, meanwhile the detection signal from Eve’s SPAD3 or SPAD4 is routed to the STOP channel of the TCSPC.

III. EXPERIMENTAL RESULTS

A. Verification of attack feasibility

In Test 1, because the trigger signals of the TCSPC and the laser pulses are synchronized, the click events recorded by the TCSPC for Eve can be precisely aligned with a specific time point within each period. We simulate Alice emitting the same polarization state $|H\rangle$, and the click events of SPAD3 ($|H\rangle$) and SPAD4 ($|V\rangle$) are recorded in the statistical histogram, as shown in Fig. 2. The zero point of the horizontal axis corresponds to the moment that Alice emits photons. A 200 ns time window is shown in Fig. 2, out of which represents only dark counts. These histograms serve as the visual representation of Eve’s detection events over time.

The red bars in Fig. 2 show the statistical results of the SPAD3 click events. The two narrower peaks on the left are attributed to backreflection from the fiber connectors. The third peak, which appears at about 250 ns, is identified as backflash photons emitted by SPAD1. In particular, the width of the peak indicates that the backflash photons probabilistically appear within a 10 ns time window, which is directly determined by the gate width of Bob’s detector. The blue bars in Fig. 2 show the statistical results of click events for SPAD4 that is configured as the other detector on the same basis as SPAD3. It is observed that there are only two peaks of backreflection, and no backflash photon is statistically shown at the expected time (around 250 ns). This is because Bob only receives the polarization state $|H\rangle$, and the backflash photons with the same state reach Eve. These backflash photons are detected only by SPAD3, while SPAD4 does not register them. The results of Test1 verify that Eve is able to estimate which Bob’s detector clicks by decoding the polarization of backflash photons, thus acquiring key

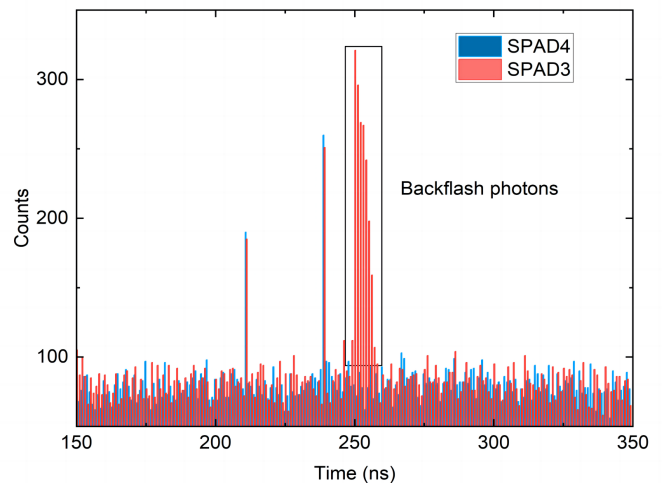


FIG. 2. Histogram of the time interval between Alice’s laser pulse emission and Eve’s detection. When the QKD system transmits the $|H\rangle$ state, the click events of Eve’s $|H\rangle$ state detector (SPAD3, red) and $|V\rangle$ state detector (SPAD4, blue) are recorded in the histogram.

information.

B. Statistical analysis of backflash photons

To quantify the threat of this attack, the most critical point is Eve’s ability to distinguish the quantum states from the backflash photons. Therefore, it is necessary to collect the counts of backflash photons from each of Eve’s detectors. Alice is configured to repeatedly prepare the same polarization state. After Bob’s detector clicked 5×10^6 times, the detected number of backflash photons was then counted, the results of which are shown in Table I. C_E means the Eve’s click counts of the SPAD in the same quantum state as Bob’s, and C_E^\perp represents the click counts of the other SPAD under the same basis but the orthogonal state. ER stands for the extinction ratio on Eve side.

TABLE I. Eve’s counts under backflash attack

Alice’s state	$ H\rangle$	$ V\rangle$	$ A\rangle$	$ D\rangle$
C_E	22526	18534	18336	18854
C_E^\perp	796	1287	741	723
ER	28.3	14.4	24.7	26.1

Table I presents the four sets of testing results for different Alice’s sending states. It can be observed from the data that when Bob emits backflash photons with a specific polarization state, the measured value of ER reached a maximum of 28.3 from numerous trials in the test. Eve’s average extinction ratio is approximately 23.4,

denoted as \overline{ER} . However, during the polarization calibration process, Eve's ER is approximately 1000 when the optical pulses are emitted from Bob. The experimental results in Table I indicate that Eve's ER for backflash photons is significantly lower than what was expected. We speculate that Eve's ability to distinguish the quantum state of backflash photons has an upper limit.

IV. SIMULATION OF BACKFLASH EXTINCTION RATIO

The parameter ER reflects Eve's ability to distinguish quantum states from the backflash photons. A higher value ER indicates that Eve can correctly decode more backflash photons. In this section, we build a theoretical simulation to explain the reasons for Eve's relatively limited ER value in the backflash attack. The detailed modeling process for different optical components is provided in Appendix A. The spectrum property of backflash photons have been shown that the wavelengths of backflash photons are widely distributed [23]. This characteristic affects Eve's decoding of backflash photons, since most devices used in the QKD system and Eve's side are sensitive to wavelengths. When backflash photons with different wavelengths pass through such wavelength-sensitive optical devices, the polarization states of photons vary, ultimately resulting in a limited ER value for Eve.

In order to quantitatively analyze the impact of the backflash photon's wide-spectrum property on the ER value, we first need to obtain the accurate wavelength distribution of the backflash photon. The spectrum of backflash photons depends mainly on the manufacturing material of the avalanche photodiode. Here we used the Ansys luminescent finite-difference time-domain (FDTD) optical simulation platform to simulate the secondary photon emission of an InGaAs avalanche photodiode and obtained the backflash photon's spectrum which is shown in Fig. 3. The wavelengths of backflash photons are distributed probabilistically between 1400 nm and 2000 nm, with the highest probability occurring near 1600 nm.

After the backflash photons are emitted from Bob's SPAD, they then pass through PBS1 and PC2 that are wavelength sensitive. When photons with different wavelengths pass through these wavelength-sensitive components, their polarizations undergo varying modifications. To establish the PBS model, we plotted the transmission curves of different wavelength photons with $|H\rangle$ polarization state as they pass through the PBS's fast and slow axes, which are shown in Fig. 6. These curves indicate that, when the wavelengths of the passing photons are inconsistent, the extinction ratio of the PBS for these photons varies. For a PC, we calculated its Jones matrix according to the actual paddle radius of the PC parameters and the number of fiber wrapped around, which are shown in Eq. (A3). In the simulation results shown in Fig. 7, we can see that the output polarization states of the $|H\rangle$ state photons with different wavelengths pass-

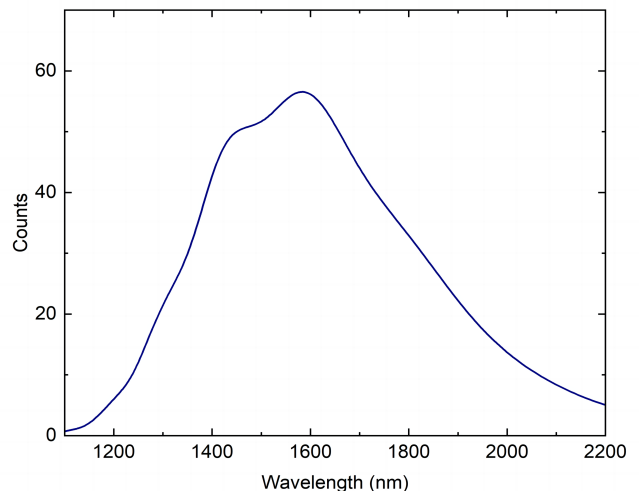


FIG. 3. The spectrum of backflash photons by using Ansys luminescent FDTD simulation platform to simulate the secondary photon emission of avalanche photodiode.

ing through the PC are different. In other words, the central wavelength of the PC depends on the angle of the paddles. For a SPAD, we modeled the detection efficiency curve for different wavelength photons, as shown in Fig. 8.

We also considered the calibration operation of PC3 as described in Sec. II B in the simulation. We set the three paddles of Bob's PC2 to a group of angles $\theta_{B_{1,2,3}}$, which encompasses the angles of three paddles, assuming that Bob can correctly decode the $|H\rangle$ and $|V\rangle$ state photons at this time. To simulate the process of adjusting the paddles for Eve θ_{E_i} ($i = 1, 2, 3$), each paddle of Eve's PC3 is scanned in steps of $\pi/50$, so PC3 has 50^3 combinations to complete a full scan of the paddle angle. In each time of the 50^3 scans, the Jones matrices of Bob's and Eve's PCs are cascaded. The $|H\rangle$ state is inputted into the cascaded matrices for calculation and performs a projection measurement on the horizontal-vertical basis. The measurement results yield probabilities $P_{|H\rangle}$ and $P_{|V\rangle}$ for the $|H\rangle$ and $|V\rangle$ states during calibration, respectively. In 50^3 iterations of computation, we select one with a $P_{|H\rangle} : P_{|V\rangle}$ about 1000: 1 (similar to the procedures in calibration operations), and the angles of three paddles of this set of PC3 are denoted as $\theta_{E_{1,2,3}}$.

Then, we simulate the procedure for detecting backflash photons. As backflash photons are emitted from a SPAD in the receiver unit, they pass through PBS1 and PC2, reaching Eve. After passing through PC3 and PBS3, the photons are finally detected by Eve's SPAD. We assume that backflash photons of different wavelengths initially carry $|H\rangle$ polarization states before entering Bob's PC2. Integrate the spectrum data of backflash photons into PC2's Jones matrix with the angle of paddles $\theta_{B_{1,2,3}}$ for calculation. It is important to note that the polarization state of the photons at each wavelength becomes distinct after passing through PC2.

Then the result of the calculation of the previous step is substituted in the Jones matrix with PC3's angle of the paddles $\theta_{E_{1,2,3}}$. The vector output from PC3 is subjected to projection measurement, yielding the measured results $P_{|H\rangle}$ and $P_{|V\rangle}$ under the backflash attack. Based on the number of backflash photons obtained from the spectrum as shown in Fig. 3 and the models of PBS and SPAD as described above, the photon numbers that Eve receives for the $|H\rangle$ and $|V\rangle$ states at each wavelength can be calculated, which are presented in Fig. 4.

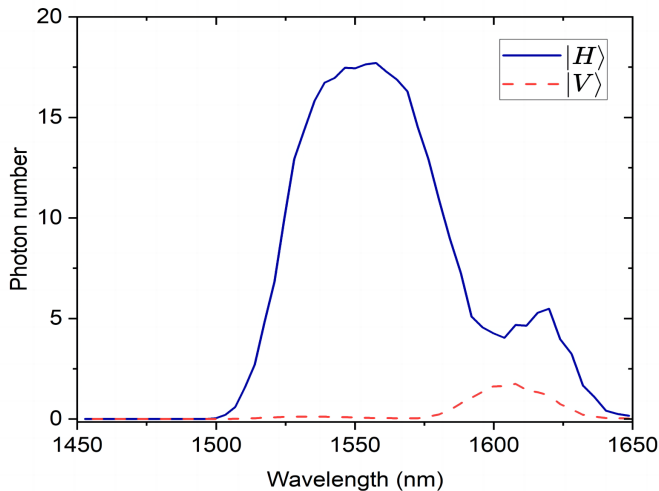


FIG. 4. The backflash photons with $|H\rangle$ polarization state undergo measurement of their polarization state by Eve after passing through PBS1, PC2, PC3, PBS2 and reaching Eve's SPAD. The blue solid line represents the number of photons decoded as $|H\rangle$ state at different wavelengths, while the red dashed line represents the number of photons decoded as $|V\rangle$ state at different wavelengths.

Finally, to calculate the ER of Eve's detection for backflash photons, one can simply sum the photon counts for each polarization across all wavelengths, as shown in Fig. 4. This allows us to calculate the ER of photons in these two polarization states. In the simulation result, the value of ER is 22, which closely matches the experimentally measured mean \overline{ER} of 23.4. When $ER = 22$, it means that Eve is able to correctly decode 95.7% of the backflash photons. That is, the ER value indicates the upper limit of Eve's capability to decode backflash photons in the QKD system and confirms the trustworthiness of our experimental data.

V. SIMULATION OF SECURE KEY RATE

In this section, we estimate the information leakage ratio attributed to the backflash attack based on the ex-

perimental data. Utilizing the ratio of information leakage, we simulate the secure key rate under the impact of the backflash attack. The theoretical simulation is based on the decoy-state BB84 QKD system [26–29], which is the scheme most commonly implemented in current QKD deployments. It is assumed that Eve only has access to obtain secret key information from decoding these backflash photons. In addition to using the signal states μ for the transmission of information between Alice and Bob, Alice also emits two decoy states characterized by distinct intensities, ν_1 and ν_2 , which satisfy $\mu > \nu_1 > \nu_2$. The Z basis is used to generate the key and the X basis is used for parameter estimation.

Generally, regarding the weak-coherent pulses emitted by Alice, there is a probability that a single pulse contains multiple photons. These multi-photon components, denoted as Δ , are considered to be insecure [30], since Eve is able to learn the information of quantum states from them. The fraction of signal states, from which Eve cannot fully obtain information, is represented as $1 - \Delta$. The secure key rate in the sifted key is estimated using the inequality as follows [31].

$$R \geq qQ_\mu[(1 - \Delta) - fH_2(\delta) - (1 - \Delta)H_2(\frac{\delta}{1 - \Delta})], \quad (1)$$

where q depends on the implementation (1/2 for the BB84 protocol due to Alice and Bob choose different bases in half of the cases, and if one uses the efficient BB84 protocol, $q \approx 1$ [32]). The Δ is expressed as $\Delta = \frac{Q_M}{Q_\mu}$, in which Q_M denotes the detection probability of Bob's detector responding to multiple-photon pulses, and Q_μ represents the overall detection probability of Bob's detector. f is the error correction efficiency. δ is the bit error rate. $H_2(x) = -x \log_2(x) - (1-x) \log_2(1-x)$ is the binary Shannon entropy function.

If Alice emits multiple photons in one pulse, we pessimistically assume that Eve intercepts at least one photon until the basis is announced and then measures it on the appropriate basis, thereby learning the key bits without introducing any error. Within the single-photon component $(1 - \Delta)$, Bob sacrifices a fraction $\frac{\delta}{1 - \Delta}$ for privacy amplification. We perform a substitution of factors in the equation, let $\frac{\delta}{1 - \Delta} = e_1$, $\Delta = \frac{Q_m}{Q_\mu}$, $1 - \Delta = \frac{Q_1}{Q_\mu}$, and $\delta = E_\mu$, where E_μ represents the overall QBER, Q_1 denotes the lower bound for the single-photon gain, and e_1 denotes the upper bound for the single-photon phase error rate. We derive the inequality for the key rate as

$$R \geq q\{-Q_\mu f(E_\mu)H_2(E_\mu) + Q_1[1 - H_2(e_1)]\}. \quad (2)$$

To estimate Y_1 and e_1 , analytical or numerical tools can be utilized. Here we employ the analytical approach proposed by Ref. [28] to evaluate the lower bound of Y_1 and the upper bound of e_1 .

$$Y_1 \geq Y_1^{L,v_1,v_2} = \frac{\mu}{\mu v_1 - \mu v_2 - v_1 + v_2} \left[Q_{v_1} e^{v_1} - Q_{v_2} e^{v_2} - \frac{v_1^2 - v_2^2}{\mu^2} (Q_\mu e^\mu - Y_0) \right], \quad (3)$$

$$e_1 \leq e_1^{\mu,v_1,v_2} = \frac{E_{v_1} Q_{v_1} e^{v_1} - E_{v_2} Q_{v_2} e^{v_2}}{(\nu_1 - \nu_2) Y_1^{L,v_1,v_2}}. \quad (4)$$

Eve is capable of implementing the backflash attack on the QKD system without interrupting its running operation. As long as Bob's SPAD experiences an avalanche, his detector exhibits a certain probability of generating backflash photons. The probability of generating backflash photons can be readily calculated as

$$P_B = \frac{N_B}{N \eta_{det} \eta_{ch}}. \quad (5)$$

In Eq. (5), η_{det} represents the detection efficiency of Eve's detector, while η_{ch} denotes the transmission rate of the channel. N_B is the number of backflash photons counted by Eve, N is the number of clicks on Bob's SPAD. In the calculation, we have counted the response N_B at Eve's detector under the fixed number of clicks at Bob's detector $N = 5 \times 10^6$ in the experiment.

Considering the wide-spectrum property of backflash photons, after they pass through the wavelength-sensitive optical device, the polarization drift causes Eve to be unable to fully decode these photons correctly. Therefore, we cannot use the total amount of backflash photons to estimate information leakage. To reflect Eve's actual decoding capability in a QKD system, we calculate the information leakage rate considering Eve's average extinction ratio \overline{ER} for the backflash photons. Therefore, the information leakage rate is

$$P_L = \left(1 - \frac{1}{\overline{ER} + 1}\right) \frac{N_B}{N \eta_{det} \eta_{ch}}, \quad (6)$$

where $\left(1 - \frac{1}{\overline{ER} + 1}\right)$ represents the proportion of backflash photons that Eve can correctly decode.

We assume that Eve is capable of receiving and storing backflash photons in a quantum memory. After the legitimate communication parties disclose their basis information, Eve selects the appropriate basis to measure the backflash photons. Among n bits of information received by Bob, there is a probability P_L that a backflash occurs and information leaks. Here, we consider the scenario most favorable to Eve, where the events of detecting backflash are solely derived from Bob's single-photon-detection events. Therefore, the sifted key is divided into three parts, $n\Delta$, nP_L , and $n(1 - \Delta - P_L)$. nP_L represents the amount of information leaked from backflash reflections. In the presence of a backflash attack, Bob sacrifices a part of the information, denoted by δ , to amplification of privacy in the segment $(1 - \Delta - nP_L)$. For the communicating parties, the components associated with multi-photon emissions and the resultant backflash

photons are both considered as security vulnerabilities,

$$n\Delta' = n\Delta + nP_L. \quad (7)$$

Replacing Δ with Δ' , the key rate under the backflash attack is given as

$$R \geq qQ_\mu \left[(1 - \Delta') - fH_2(\delta) - (1 - \Delta')H_2\left(\frac{\delta}{1 - \Delta'}\right) \right]. \quad (8)$$

TABLE II. Experimental parameters used in simulations.

Parameter	Value
Channel loss coefficient (dB/km)	$\alpha = 0.2$
Dark count rate	$P_d = 10^{-5}/gate$
Total misalignment error	$e_d = 1\%$
Detection efficiency of the SPADs	$\eta_D = 12.5\%$
Error correction efficiency	$f = 1.12$

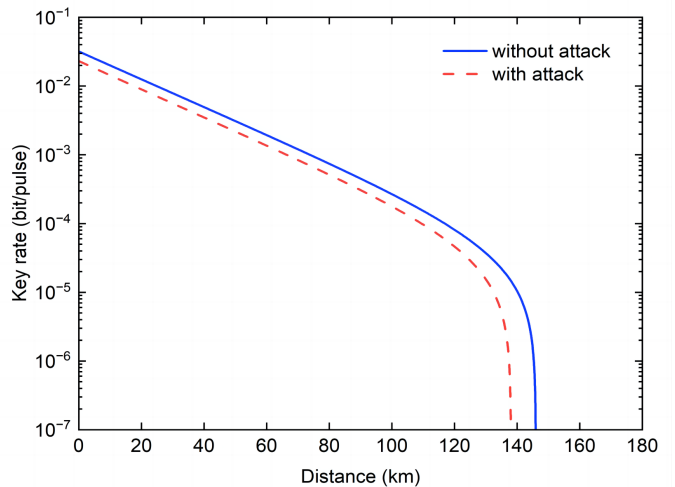


FIG. 5. Simulation results based on decoy state BB84-QKD protocol. The solid blue line is the key rate curve without backflash attack, and the dashed red line is the key rate curve under backflash attack.

Using the experimental parameters listed in Table II, the resulting lower bounds of the key rate are depicted in Fig. 5. The solid blue line indicates the lower bound of the key rate, R , as stipulated by Eq. (2) in the absence of

the backflash attack. Herein, for each specified distance, we determine the optimal intensities of μ_s , ν_1 , and ν_2 to maximize R . Subsequently, according to Eq. (8), we simulate the lower bound of the key rate R' under backflash attack, which is represented by the red dashed curve, as shown in Fig. 5. It is evident that the key rate R' under the backflash attack is significantly lower than R without the attack. In our simulated key rate model, the maximum transmission distance decreased from 146 km to 138 km affected by the backflash attack. We theoretically prove that the security of QKD is compromised due to the presence of the backflash attack.

VI. CONCLUSION

In this paper, we study the effect of the backflash attack on fiber-based QKD systems. We verified the feasibility of Eve obtaining key information through backflash photons. Eve's decoding capability is reflected in her ER of polarization states for backflash photons, which is approximately 23.4 in average obtained from the experimental testing. The relatively low ER is due to polarization drift caused by wavelength inconsistencies of backflash photons as they pass through wavelength-sensitive components, which we have validated through theoretical simulation. Based on Eve's decoding ability, we simulated the secure key rate, which clearly shows that the security is compromised by the backflash attack. This work provides a general methodology to experimentally and theoretically quantify the upper limit of backflash attack on a decoy-state BB84 QKD system.

ACKNOWLEDGMENTS

We thank Yaxuan Wang and Tianyi Xing for discussions. This work was funded by the National Natural Science Foundation of China (No. 62371459) and the Innovation Program for Quantum Science and Technology (2021ZD0300704).

Appendix A: Optical device modeling

The spectrum of backflash photon is distributed across a certain frequency range. Most of the optical devices through which photons pass are wavelength-sensitive. Simulating by modeling the devices helps to explain the phenomenon of low ER value in Eve's polarization decoding.

We used the Ansys Lumerical FDTD photonic simulation platform for avalanche photodiode simulation. The platform provides a secondary photon emission model for InGaAs avalanche photodiodes and allows us to configure relevant parameters, including materials, thickness, and light source. Then, a monitor is added to detect the secondary photon emission from the avalanche diode and

obtain its backflash spectrum. The backflash spectrum is shown in Fig. 3.

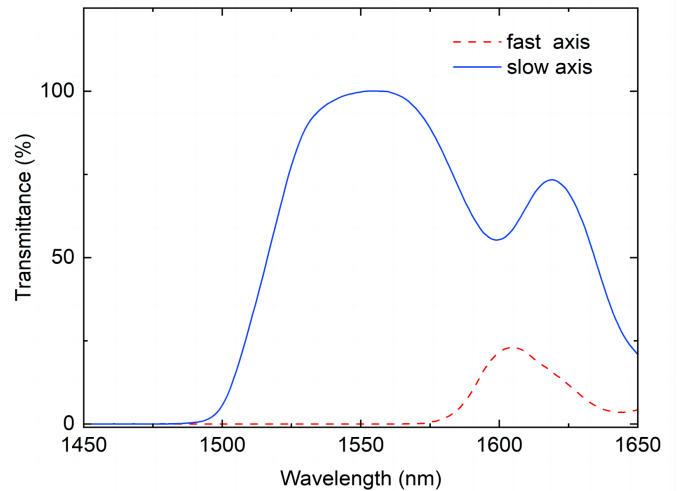


FIG. 6. The transmittance of different wavelengths in the two paths of a PBS. The blue solid line represents the transmittance of the $|H\rangle$ state through the slow axis, while the red dashed line represents the transmittance of the $|H\rangle$ state through the fast axis.

Figure 6 shows a PBS with a central wavelength of 1550 nm, where the transmittance through the fast axis and the slow axis varies for different wavelengths of photons. Around 1600 nm, the transmittance for the fast-axis and slow-axis shows a compensating trend, which, from Eve's perspective, there is a certain probability of decoding into a wrong quantum state, which will increase the bit error for her.

The 3-Paddle Polarization Controller utilizes stress-induced birefringence to create three independent fractional wave plates to alter the polarization in single-mode fiber that is looped around three independent spools (fiber retarders). The amount of birefringence induced in the fiber is a function of the fiber cladding diameter, the spool diameter (fixed), the number of fiber loops per spool, and the wavelength of the photons. The fast axis of the fiber, which is in the plane of the spool, is adjusted with respect to the transmitted polarization vector by manually rotating the paddles to twist the fiber. To transform an arbitrary input polarization state into another arbitrary output polarization state, a combination of three paddles (a quarter-wave plate, a half-wave plate, and a quarter-wave plate) can be used. The retardance of each paddle may be estimated from the following equation:

$$\varphi(\text{Radians}) = \frac{2\pi^2 a N d^2}{\lambda D}, \quad (\text{A1})$$

$$\varphi(\text{Waves}) = \frac{\pi a N d^2}{\lambda D}. \quad (\text{A2})$$

In the formula, φ is the phase retardance, a is a constant (for quartz fiber, a equals 0.133), N is the number of fiber

loops, d is the diameter of the fiber cladding, λ is the wavelength, and D is the diameter of the paddle. As can be seen from Eq. (A1), Eq. (A2), the influence of PC on phase retardance changes depends on the wavelength of the input photons. Assuming that photons with unique

initial polarization states but different wavelengths enter the PC, the PC changes the different phase retardances for the various wavelengths of photons. List the Jones matrices for the polarization effects of the three paddles:

$$\begin{aligned} U_{\theta_1}(\varphi_1) &= \begin{pmatrix} \cos\theta_1 & -\sin\theta_1 \\ \sin\theta_1 & \cos\theta_1 \end{pmatrix} \begin{pmatrix} e^{j\frac{\varphi_1}{2}} & 0 \\ 0 & e^{-j\frac{\varphi_1}{2}} \end{pmatrix} \begin{pmatrix} \cos\theta_1 & \sin\theta_1 \\ -\sin\theta_1 & \cos\theta_1 \end{pmatrix}, \\ U_{\theta_2}(\varphi_2) &= \begin{pmatrix} \cos\theta_2 & -\sin\theta_2 \\ \sin\theta_2 & \cos\theta_2 \end{pmatrix} \begin{pmatrix} e^{j\frac{\varphi_2}{2}} & 0 \\ 0 & e^{-j\frac{\varphi_2}{2}} \end{pmatrix} \begin{pmatrix} \cos\theta_2 & \sin\theta_2 \\ -\sin\theta_2 & \cos\theta_2 \end{pmatrix}, \\ U_{\theta_3}(\varphi_3) &= \begin{pmatrix} \cos\theta_3 & -\sin\theta_3 \\ \sin\theta_3 & \cos\theta_3 \end{pmatrix} \begin{pmatrix} e^{j\frac{\varphi_3}{2}} & 0 \\ 0 & e^{-j\frac{\varphi_3}{2}} \end{pmatrix} \begin{pmatrix} \cos\theta_3 & \sin\theta_3 \\ -\sin\theta_3 & \cos\theta_3 \end{pmatrix}. \end{aligned} \quad (\text{A3})$$

In each equation, U represents the Jones matrix of the PC's paddle, which is related to the paddle's angle of rotation. Three formulas represent three paddles. By cascading these matrices, the PC's simulation model can be constructed.

In the polarization controller model, a 1550 nm photon with arbitrary polarization is used as the input photon, the angles of the paddles are adjusted to ensure that the output polarization state is $|H\rangle$. By fixing the angles of the paddles, we change the wavelength of the input photons and measure the polarization state of the output photons. The probability of the measurement results being $|H\rangle$ is calculated as shown in Fig. 7. In Fig. 7, the

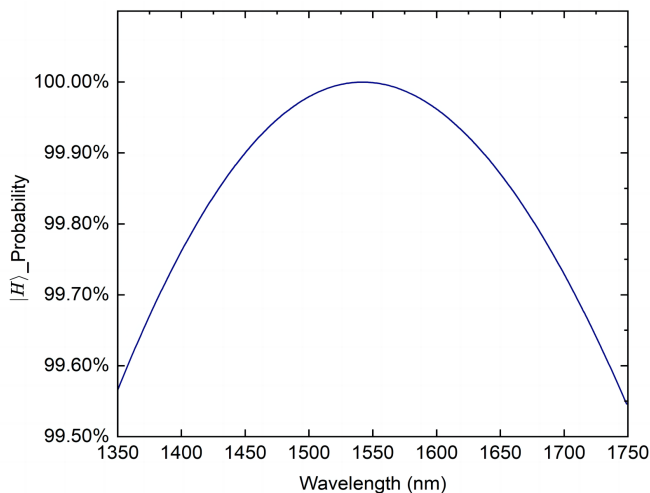


FIG. 7. The probability of photons with different wavelengths being measured in the $|H\rangle$ state after passing through the polarization controller with the paddle fixed.

horizontal axis represents the wavelength of the input

photons, while the vertical axis shows the probability of obtaining the polarization state $|H\rangle$ of the output photons. The angle of the PC paddles is set using input photons of 1550 nm, so the PC is optimized to adjust the photons in 1550 nm to the state $|H\rangle$. The simulation results confirm the wavelength sensitivity of the PC.

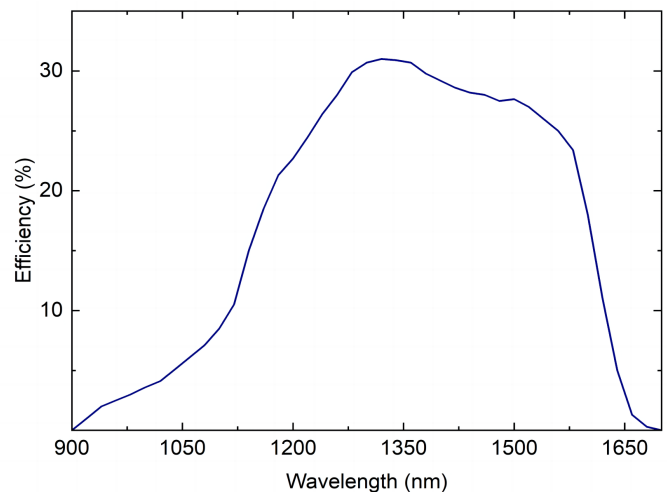


FIG. 8. The detection efficiency of a SPAD for photons with different wavelengths.

The curve in Fig. 8 represents the detection efficiency of SPAD at various wavelengths. For Bob, the efficiency of SPAD corresponds to a specific point in Fig. 8, where the detection probability of the 1550 nm photons is 25%. For Eve, the SPAD efficiency corresponds to a segment of the curve in Fig. 8. As backflash photons of different wavelengths reach Eve's detector, the efficiency of detecting varies.

[1] P. W. Shor , Polynomial-time algorithms for prime factorization and discrete logarithms on a quantum com-

puter , in *SIAM Review* 41, 303 (1999).

- [2] P. W. Shor, Algorithms for quantum computation: discrete logarithms and factoring, in *Proceedings 35th Annual Symposium on Foundations of Computer Science* (1994).
- [3] Zbinden, H and Gisin, N and Ribordy, G and Stucki, D and Tittel, W, Experimental quantum communication, in *Experimental Quantum Computation and Information* (2002).
- [4] V. Scarani, H. Bechmann-Pasquinucci, N. J. Cerf, M. Dušek, N. Lutkenhaus, and M. Peev, The security of practical quantum key distribution, in *Rev. Mod. Phys.* *81*, 1301 (2009).
- [5] Lo, Hoi-Kwong and Curty, Marcos and Tamaki, Kiyoshi, Secure quantum key distribution, in *Nat. Photonics* *8*, 595 (2014).
- [6] Makarov, Vadim and Anisimov, Andrey and Skaar, Johannes, Effects of detector efficiency mismatch on security of quantum cryptosystems, in *Phys. Rev. A* *74*, 022313 (2006).
- [7] L. Lydersen, C. Wiechers, C. Wittmann, D. Elser, J. Skaar, and V. Makarov, Hacking commercial quantum cryptography systems by tailored bright illumination, in *Nat. Photonics* *4*, 686 (2010).
- [8] I. Gerhardt, Q. Liu, A. Lamas-Linares, J. Skaar, C. Kurtz, and V. Makarov, Full-field implementation of a perfect eavesdropper on a quantum cryptography system, in *Nat. Commun* *2*, 349 (2011).
- [9] V. Chistiakov, A. Huang, V. Egorov, and V. Makarov, Controlling single-photon detector ID210 with bright light, in *Opt. Express* *27*, 32253 (2019).
- [10] A. Huang, A. Navarrete, S.-H. Sun, P. Chaiwongkhot, M. Curty, and V. Makarov, Laser-Seeding Attack in Quantum Key Distribution, in *Phys. Rev. Appl.* *12*, 064043 (2019).
- [11] A. Huang, R. Li, V. Egorov, S. Tchouragoulov, K. Kumar, and V. Makarov, Laser-Damage Attack Against Optical Attenuators in Quantum Key Distribution, in *Phys. Rev. Appl.* *13*, 034017 (2020).
- [12] Z. Wu, A. Huang, H. Chen, S.-H. Sun, J. Ding, X. Qiang, X. Fu, P. Xu, and J. Wu, Hacking single-photon avalanche detectors in quantum key distribution via pulse illumination, in *Opt. Express* *28*, 25574 (2020).
- [13] A. Ponosova, D. Ruzhitskaya, P. Chaiwongkhot, V. Egorov, V. Makarov, and A. Huang, Protecting Fiber-Optic Quantum Key Distribution Sources against Light-Injection Attacks, in *PRX Quantum* *3*, 040307 (2022).
- [14] A. Huang, A. Mizutani, H.-K. Lo, V. Makarov, and K. Tamaki, Characterization of State-Preparation Uncertainty in Quantum Key Distribution, in *Phys. Rev. Appl.* *19*, 014048 (2023).
- [15] Q. Peng, B. Gao, K. Zaitsev, D. Wang, J. Ding, Y. Liu, Q. Liao, Y. Guo, A. Huang, and J. Wu, Practical security of twin-field quantum key distribution under wavelength-switching attack, in *arXiv:2408.09318*.
- [16] Q. Peng, J.-P. Chen, T. Xing, D. Wang, Y. Wang, Y. Liu, and A. Huang, Practical security of twin-field quantum key distribution under wavelength-switching attack, in *arXiv:2408.09318*.
- [17] A. Huang, S. Sajeed, P. Chaiwongkhot, M. Soucarros, M. Legré, and V. Makarov, Testing Random-Detector-Efficiency Countermeasure in a Commercial System Reveals a Breakable Unrealistic Assumption, in *IEEE J. of Quantum Electronics* *52*, 1 (2016).
- [18] B. Gao, Z. Wu, W. Shi, Y. Liu, D. Wang, C. Yu, A. Huang, and J. Wu, Ability of strong-pulse illumination to hack self-differencing avalanche photodiode detectors in a high-speed quantum-key-distribution system, in *Phys. Rev. A* *106*, 033713 (2022).
- [19] C. Wiechers, L. Lydersen, C. Wittmann, D. Elser, J. Skaar, C. Marquardt, V. Makarov, and G. Leuchs, After-gate attack on a quantum cryptosystem, in *New J. Phys* *13*, 013043 (2011).
- [20] Y. Zhao, C.-H. F. Fung, B. Qi, C. Chen, and H.-K. Lo, Quantum hacking: Experimental demonstration of time-shift attack against practical quantum-key-distribution systems, in *Phys. Rev. A* *78*, 042333 (2008).
- [21] A. Meda, I. Degiovanni, A. Tosi, Z. Yuan, G. Brida, and M. Genovese, Quantum key distribution security threat: the backflash light case, in *Quantum Technologies 2018 pp. 138-144* (2018).
- [22] A. Koehler-Sidki, J. F. Dynes, T. K. Parařiso, M. Lucamarini, A. W. Sharpe, Z. L. Yuan, and A. J. Shields, Backflashes from fast-gated avalanche photodiodes in quantum key distribution, in *APL* *116*, 154001 (2020).
- [23] A. Meda, I. P. Degiovanni, A. Tosi, Z. Yuan, G. Brida, and M. Genovese, Quantifying backflash radiation to prevent zero-error attacks in quantum key distribution, in *LSA* *6*, e16261 (2017).
- [24] P. V. P. Pinheiro, P. Chaiwongkhot, S. Sajeed, R. T. Horn, J.-P. Bourgoin, T. Jennewein, N. Lutkenhaus, and V. Makarov, Eavesdropping and countermeasures for backflash side channel in quantum cryptography, in *Opt. Express* *26*, 21020 (2018).
- [25] Chynoweth, A. G. and McKay, K. G., Photon Emission from Avalanche Breakdown in Silicon, in *Phys. Rev.* *102*, 369 (1956).
- [26] Wang, Xiang-Bin, Beating the Photon-Number-Splitting Attack in Practical Quantum Cryptography, in *Phys. Rev. Lett.* *94*, 230503 (2005).
- [27] H.-K. Lo, X. Ma, and K. Chen, Decoy State Quantum Key Distribution, in *Phys. Rev. Lett.* *94*, 230504 (2005).
- [28] Ma, Xiongfeng and Qi, Bing and Zhao, Yi and Lo, Hoi-Kwong, Practical decoy state for quantum key distribution, in *Phys. Rev. A* (2005).
- [29] X.-B. Wang, C.-Z. Peng, J. Zhang, L. Yang, and J.-W. Pan, General theory of decoy-state quantum cryptography with source errors, in *Phys. Rev. A* *77*, 042311 (2008).
- [30] B. Huttner, N. Imoto, N. Gisin, and T. Mor, Quantum cryptography with coherent states, in *Phys. Rev. A* *51*, 1863 (1995).
- [31] D. Gottesman, H.-K. Lo, N. Lutkenhaus, and J. Preskill, Security of quantum key distribution with imperfect devices, in *International Symposium on Information Theory, 2004. ISIT 2004. Proceedings.* (2004).
- [32] H.-K. Lo, H. F. Chau, and M. Ardehali, Efficient quantum key distribution scheme and a proof of its unconditional security, in *J. Cryptol* *18*, 133 (200).